Astronomy & Astrophysics manuscript no. 3268 February 5, 2008
(DOI: will be inserted by hand later)

An infrared study of galactic OH/IR stars. II. The 'GLMP sample' of red oxygen-rich AGB stars

F. M. Jiménez-Esteban[1,3], P. García-Lario[2], D. Engels[3], and J.V. Perea Calderón[1]

[1] ISO Data Centre / European Space Astronomy Center, Villafranca del Castillo, Apartado de Correos 50727, E-28080 Madrid, Spain.
[2] ISO Data Centre / European Space Astronomy Center, Research and Scientific Support Department of ESA, Villafranca del Castillo, Apartado de Correos 50727, E-28080 Madrid, Spain.
[3] Hamburger Sternwarte, Gojenbergsweg 112, D-21029 Hamburg, Germany.

Received 20 April 2005 / Accepted 26 July 2005

Abstract.
We present optical and near-infrared finding charts taken from the DSS and 2MASS surveys of 94 IRAS sources selected from the GLMP catalogue, and accurate astrometry ($\approx 0.2''$) for most of them. Selection criteria were very red IRAS colours representative for OH/IR stars with optically thick circumstellar shells and the presence of variability according to the IRAS variability index (VAR>50). The main photometric properties of the stars in this 'GLMP sample' are presented, discussed and compared with the correspondent properties of the 'Arecibo sample' of OH/IR stars studied nearlier. We find that 37% of the sample (N = 34) has no counterpart in the 2MASS, implying extremely high optical depths of their shells. Most of the sources identified in the 2MASS are faint (K$\gtrsim$8) and are of very red colour in the near-infrared, as expected. The brightest 2MASS counterpart (K=5.3 mag) was found for IRAS 18299–1705. Its blue colour H–K=1.3 suggests that IRAS 18299–1705 is a post-AGB star. Few GLMP sources have faint but relatively blue counterparts. They might be misidentifed field stars or stars that recently experienced a drop of their mass loss rates. The 'GLMP sample' in general is made of oxygen-rich AGB stars, which are highly obscured by their circumstellar shells. They belong to the same population as the reddest OH/IR stars in the 'Arecibo sample'.

Key words. Stars: OH/IR – Stars: AGB and post-AGB – Stars: circumstellar matter – Stars: variable – Stars: evolution – Infrared: stars

1. Introduction

This is the second of a series of three papers devoted to the study of galactic OH/IR stars. In the first two papers we characterize in the optical and in the near-infrared two large samples of OH/IR stars: the 'Arecibo sample' studied in Jiménez-Esteban et al. 2005a (hereafter Paper I), and the 'GLMP sample' studied here. In a forthcoming paper (Jiménez-Esteban et al. 2005b; Paper III) we combine both samples to study the origin of the long-spread sequence of far-infrared colours found by IRAS for oxygen-rich AGB stars, and propose evolutionary links between the various classes of AGB stars and Planetary Nebulae identified in our Galaxy.

In Paper I we discussed the main optical/near-infrared properties of a well-defined sample of far-infrared selected AGB stars showing OH maser emission. This sample, the 'Arecibo sample', consists of 385 IRAS sources, which were detected in the 1612 MHz OH maser line with the Arecibo radio telescope (Eder et al. 1988; Lewis et al. 1990; Chengalur et al. 1993). The sample was obtained from a complete survey of IRAS sources with flux densities ≥ 2 Jy at 25 μm, with declination $0 < \delta < 37^\circ$ and appropriate colours of AGB stars (Olnon et al. 1984). The OH maser detections qualify the IRAS sources as O-rich AGB stars. This sample is mainly constituted by optically visible sources ($\approx 2/3$ of the sample), having optically thin circumstellar envelopes (CSE), and by a smaller contribution of optically invisible ones ($\approx 1/3$ of the sample), having thick CSEs. These OH/IR stars are distributed over a wide range of the near-infrared J-H vs. H-K colour-colour diagram, which was shown in Paper I to be an extension toward redder colours of the area where optically visible Mira variables are normally found (Whitelock et al. 1994).

The 'Arecibo sample' predominantly represents the bluer (and probably less massive) population of galactic OH/IR stars. A minority of highly obscured OH/IR star is present. To increase the sample of such OH/IR stars we compiled a new sample, taken this time from the GLMP catalogue (García-Lario 1992). The purpose of the following analysis is to determine the optical/near-infrared properties of this sample of very red (and probably of higher mass) AGB stars, and to establish con-

Send offprint requests to: F.M. Jiménez-Esteban,
e-mail: Francisco.Jimenez-Esteban@hs.uni-hamburg.de

Table 1. Objects in common to the GLMP catalogue and to the 'Arecibo sample'

GLMP	IRAS	GLMP	IRAS
842	18517+0037	851	18549+0208
876	19065+0832	877	19067+0811
882	19081+0322	901	19183+1148
902	19188+1057	920	19283+1944
934	19352+2030	939	19374+1626
958	19565+3140	960	19576+2814
966	20023+2855	972	20043+2653
983	20137+2838	999	20272+3535

nections with the properties of the 'Arecibo sample'. In a similar way as we did for the Arecibo sources we have created an atlas of finding charts combining optical images from the Second Digitized Sky Survey (DSS2; Djorgovski et al. 2001) and near-infrared images from the Two Micron All Sky Survey (2MASS; Cutri et al. 2003).

Section 2 contains a description of the selected sample. In Section 3 the process of identification of the optical/near-infrared counterparts is explained. This is followed by a brief description of the atlas contents. The results obtained are discussed in Section 4. The main conclusions are presented in Section 5.

2. Sample selection

The GLMP catalogue (García-Lario 1992) contains 1084 IRAS sources with [12]–[25] vs. [25]–[60] colours similar to those shown by planetary nebulae (PNe). To include an object in this catalogue the source must have been well detected (IRAS-FQual ≥ 2) in at least the three IRAS photometric bands centred at 12, 25 and 60 μm and obey the following constraints:

i) $F_\nu(12\mu m)/F_\nu(25\mu m) \leq 0.50$

ii) $F_\nu(25\mu m)/F_\nu(60\mu m) \geq 0.35$

iii) $F_\nu(60\mu m)/F_\nu(100\mu m) \geq 0.60$, if a reliable measurement (IRAS-FQual ≥ 2) was available in the 100 μm band.

Thus, the GLMP catalogue is made up by a heterogeneous collection of far-infrared selected sources distributed over the full sky with very red IRAS colours ([12]–[25] ≥ 0.75), containing PNe, but also a considerable number of AGB and post-AGB stars (apart from a small percentage of 'contaminant' sources like T-Tauri stars, Herbig Ae-Be stars, ultracompact H II regions and even a few Seyfert galaxies). To identify the O-rich AGB stars among them, we selected objects located in a characteristic region of the IRAS two-colour diagram along the sequence of colours predicted for O-rich AGB stars with increasing mass loss (Bedijn 1987; in the following we will name this path the 'O-rich AGB sequence') (see Fig. 1) having a high (VAR > 50) IRAS variability index. They are classified in the GLMP catalogue as 'variable OH/IR stars'. Indeed, most but not all of these stars have OH maser detections at 1612 MHz and are therefore genuine OH/IR stars. The rest was either never observed in OH or not detected. Nevertheless, they were classified by García-Lario as 'variable OH/IR stars', in accordance with Lewis (1992), who found that these stars called by him 'OH/IR star mimics' are indeed O-rich variable AGB stars.

Two sources with low VAR index, namely IRAS 11438–6330 and IRAS 12358–6323, were included in addition because near infrared photometric observations taken from the literature confirmed that both objects are strongly variable in the near-infrared (Gaylard et al. 1989; Lepine et al. 1995; Hu et al. 1993; García-Lario et al. 1997) and, thus, can also be considered as 'variable OH/IR stars'.

The variability cut, while efficient in excluding non-AGB objects, introduces a bias. Only $\approx 70\%$ of the sky was surveyed three times during the IRAS mission, while 20% was observed only twice, and thus the variable sources in some parts of the sky were more likely recognized than others. Furthermore, the variability detection significantly depends on colour. Due to the short lifetime of the IRAS satellite ($\approx$10 months), it was more probable to observe variability in OH/IR stars with shorter periods (bluer IRAS colours) than in those with longer periods (redder IRAS colours).

The selected sources form a group of 110 OH/IR stars of which 16 are also part of the 'Arecibo sample' of OH/IR stars (see Table 1). Since the optical/near-infrared characteristics of the sources in the 'Arecibo sample' were already presented and discussed in Paper I, we have not analysed again the objects in common. Then, after these are excluded, the resulting 'GLMP sample' is formed by a total of 94 OH/IR stars with very red IRAS colours.

The position of the 'GLMP sample' in the IRAS two-colour diagram is shown in Fig. 1, together with the 'O-rich AGB sequence', and the position of the 'Arecibo sample'. The 'GLMP sample' occupies the red part in this diagram, increasing considerably the number of objects classified as OH/IR stars or O-rich AGB stars in this color range.

3. Identification of the optical/IR counterparts

In order to determine the optical/near infrared counterparts of the 94 OH/IR stars in our sample we first determined the best coordinates available from existing catalogues and then searched for plausible counterparts at these locations both on the near-infrared images taken from the 2MASS and on the optical images taken from the DSS2.

3.1. Cross-correlation with the MSX

Improved coordinates with respect to those originally provided by the IRAS Point Source Catalogue (accuracy typically between $10'' - 15''$) can be obtained by cross-correlating our sample with the MSX Point Source Catalogue (MSX6C) (Egan et al. 2003), which provides coordinates of the mid-infrared counterparts with an accuracy of $\approx 2''$. The MSX survey is limited to low galactic latitudes ($\leq |6|^\circ$) and, therefore, not all GLMP sources have an associated MSX entry. However, the accuracy of the MSX positions is in many cases essential to identify the near-infrared counterpart, in particular in crowded regions along the galactic plane and/or close to the Galactic Centre, and

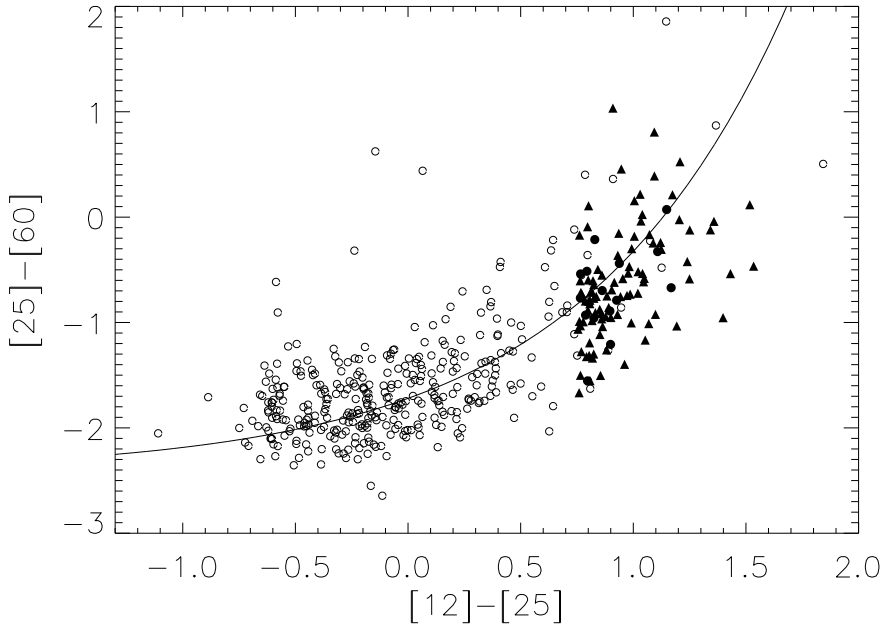

Fig. 1. The position in the IRAS two-colour diagram of OH/IR stars in the 'GLMP sample' (filled triangles) is compared with the position of the OH/IR stars in the 'Arecibo sample' (open circles). Filled circles are used for the few objects in common. The solid line is the 'O-rich AGB sequence' (see text), and the IRAS colours are defined as: $[12]-[25] = -2.5 \log \frac{F_\nu(12)}{F_\nu(25)}$ and $[25]-[60] = -2.5 \log \frac{F_\nu(25)}{F_\nu(60)}$.

for extremely red objects only marginally detectable in the K band.

We searched for the MSX counterpart in an area of 60″ radius around the original IRAS position. When more than one MSX source was found, we selected the reddest MSX counterpart, because only the reddest sources show MSX photometric data consistent with the IRAS photometry. In almost all cases the reddest MSX counterpart was also the nearest with respect to the search position.

Out of a total of 85 objects located within the MSX sky survey area, we found that 82 objects (96% of them) had a plausible mid-infrared counterpart in the MSX6C (see Tables 3 and 4). This high rate is similar to that found for the 'Arecibo sample' (Paper I). The 3 sources without MSX counterpart were probably missed because they are located at the edges of the MSX survey area, at galactic latitudes $|b| > 5.3°$. For these 3 sources, plus the 9 additional ones not covered by MSX, we could not improve the original IRAS astrometry.

3.2. 2MASS near-infrared counterparts

3.2.1. General search method

Near-infrared counterparts were searched for in the Two Micron All Sky Survey (2MASS). We first inspected the 2MASS images and obtained the position and the photometry of the selected counterpart mostly from the 2MASS Point Source Catalogue (2MASS-PSC), which has an astrometric accuracy of $\approx 0.2''$. Depending on whether the coordinates were from IRAS or from MSX, we inspected a circle with radius 30″ or 6″, respectively, centered on the nominal source position and searched for a plausible (i.e. redder than average) counterpart. In approximately one third of the cases only one source was found showing redder than average colours. In another third of the cases more than one red object was found. We always selected the redder object, which turned out to be also the nearest with two exceptions: IRAS 17392–3020 and IRAS 19087+1006.

Not all near-infrared counterparts identified were actually included in the 2MASS-PSC. Five of them were identified directly on the 2MASS images. These counterparts were probably not included in the PSC because of blending with nearby sources or due to insufficient signal-to-noise ratio. For example, close to the MSX position of IRAS 17151–3642 only a very bright source (2MASS 259.622353–36.768497) was listed in the PSC, while on the images an additional object invisible in the J-band appears on the H- and K-band images very close to the bright source. This very red object was selected then as the most reliable counterpart. A similar case is IRAS 17495–2534. The near-infrared counterparts of IRAS 17428–2438 and IRAS 18091–2437 are faint and only visible in the K-band, probably with a flux below the detectability threshold. Finally, IRAS 18182–1504 is clearly in H- and K-band images, but there is no entry in the 2MASS-PSC. For all these sources we derived their astrometric coordinates directly from the 2MASS

images by determining the centroid of the point-like emission associated with the near-infrared counterpart.

A peculiar case is IRAS 18000–2835. One 2MASS counterpart is located only ≈ 1.8″ off the MSX position, and shows the strongest (K = 5.05) near-infrared brightness in the sample, although with relatively blue colors (H–K = 0.7). A second 2MASS counterpart was found in addition ≈ 3.8″ off the MSX position, also showing strong (K = 7.14) near-infrared brightness, but with redder colours (H–K = 1.4). From the confusion flags quoted by the 2MASS-PSC for these two sources it follows that the photometry of both stars is contaminated. They may be a binary system, as there is very little chance to find two such bright stars so close together. Because of the low spatial resolution of the IRAS satellite, it is possible that the IRAS 18000–2835 fluxes are a combination of the individual fluxes of both stars. Furthermore, this source was not detected in the 1612 MHz OH maser line by te Lintel Hekkert (1991) which leaves its classification as an oxygen-rich AGB star open. Therefore, we omitted IRAS 18000–2835 from the following discussions.

65 2MASS near-infrared candidate counterparts were found by this method among the now 81 IRAS sources with MSX identifications, while in 16 cases (20% of the sources with associated MSX counterparts) no object was found. Out of the 12 objects without MSX coordinates we were able to find suitable near-infrared candidate counterparts in ten cases. IRAS 18195–2804 and IRAS 18479–2514 did not show any plausible counterpart in the 2MASS.

3.2.2. Constraints due to contamination by field stars

Among the candidate counterparts a surprisingly large fraction did not show the extremely red near-infrared colors expected for this sample. This is shown in Figure 2, where we have plotted the near-infrared colour H–K as a function of K magnitude for all 2MASS candidate counterparts with near-infrared photometry available. For comparison also the 'Arecibo sample' is plotted. For the sources not detected in H, lower limits for the H–K colour were calculated and marked with vertical arrows.

A general correlation exists between the H–K colour and the K magnitude for the 'Arecibo sample', although there is a large scatter in both axes. This distribution was explained in Paper I by an increase of optical thickness of the CSEs (increase of H–K colour) leading to an increase of obscuration in the near-infrared (decrease in K-band brightness). The scatter is the result of i) the strong variability with typical amplitudes $1^m \lesssim \Delta K \lesssim 2^m$ rising in the most extreme cases up to 4^m; and ii) the range of distances of 1–5 kpc (Paper III), and iii) the variability of H–K colours which can reach Δ (H–K) $\geq 1^m$ (Harvey et al. 1974; Engels et al. 1983; Jiménez-Esteban et al. 2005c).

Only part of the 2MASS candidate counterparts follow the general correlation shown by the 'Arecibo sample'. They are located to the left of the dashed line in Figure 2, which was fitted by eye to outline the lower limits of H–K colours of the 'Arecibo sample'. Hereafter this group of counterparts is referred to as the 'red subsample'. For K > 9 many 2MASS candidate counterparts (as well as three of the 'Arecibo sample') are surprisingly blue with H–K $\lesssim$ 2 (to the right of the dashed line in Figure 2; hereafter 'blue subsample'). These candidates do not follow the correlation of redder colours with fainter K–band brightness.

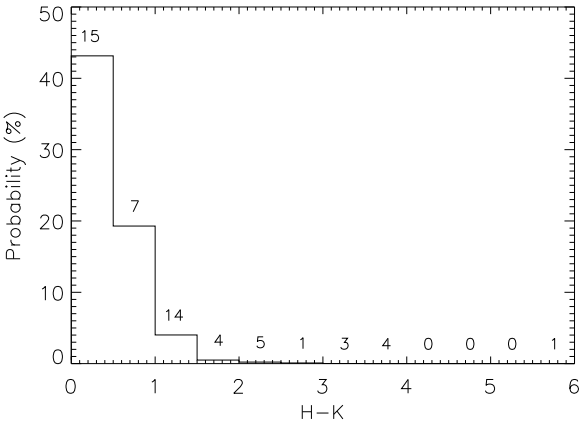

Fig. 3. Probability of finding a field star within the search area as a function of the near-infrared H–K colour. The rate of 2MASS candidate counterparts actually found is given in percentage on top of each bin.

A possible explanation for the objects of the 'blue subsample' is misidentification with field stars. Despite a relatively small search box for the majority of the sources, the probability of misidentification is not negligible. The stellar fields were in many cases very crowded since some of them correspond to regions of very low galactic latitude and/or are located in the direction of the Galactic Center. Then, more than one 2MASS point source was usually (≈ 30%) found within the search area.

In order to quantify the contamination we determined the probability of misidentifications as a function of the H–K colour. We randomly selected 9 fields in the vicinity of GLMP sources and collected all 2MASS_PSC entries with H- and K-band detections within a radius of < 2.5′ from their MSX coordinates. With a total number of ≈ 4 000 sources, we calculated the probability to find a field star within a circle of 6″ as function of the H–K colour. The result is shown in Figure 3.

If we now consider the whole sample of GLMP sources, we can see that they follow a different colour distribution, showing much redder H–K colours in general than expected from the probability analysis. The percentage of 2MASS candidate counterparts actually found is given on top of each colour bin in Figure 3. This clearly suggests that the probability of misidentification is negligible for the redder counterparts. The chance to find a field star with H–K ≥ 1.5 is below 1%, while we find that 18% of the 2MASS candidate counterparts show such red colours. Thus, all of them can be considered as plausible counterparts, irrespective their compliance with the general correlation shown by the 'Arecibo sample'.

The 2MASS candidate counterparts with H–K < 1.0 can be explained completely as misidentifications with field stars, in accordance with the results obtained from the 'Arecibo sample'. In Paper I we showed that the handful of Arecibo

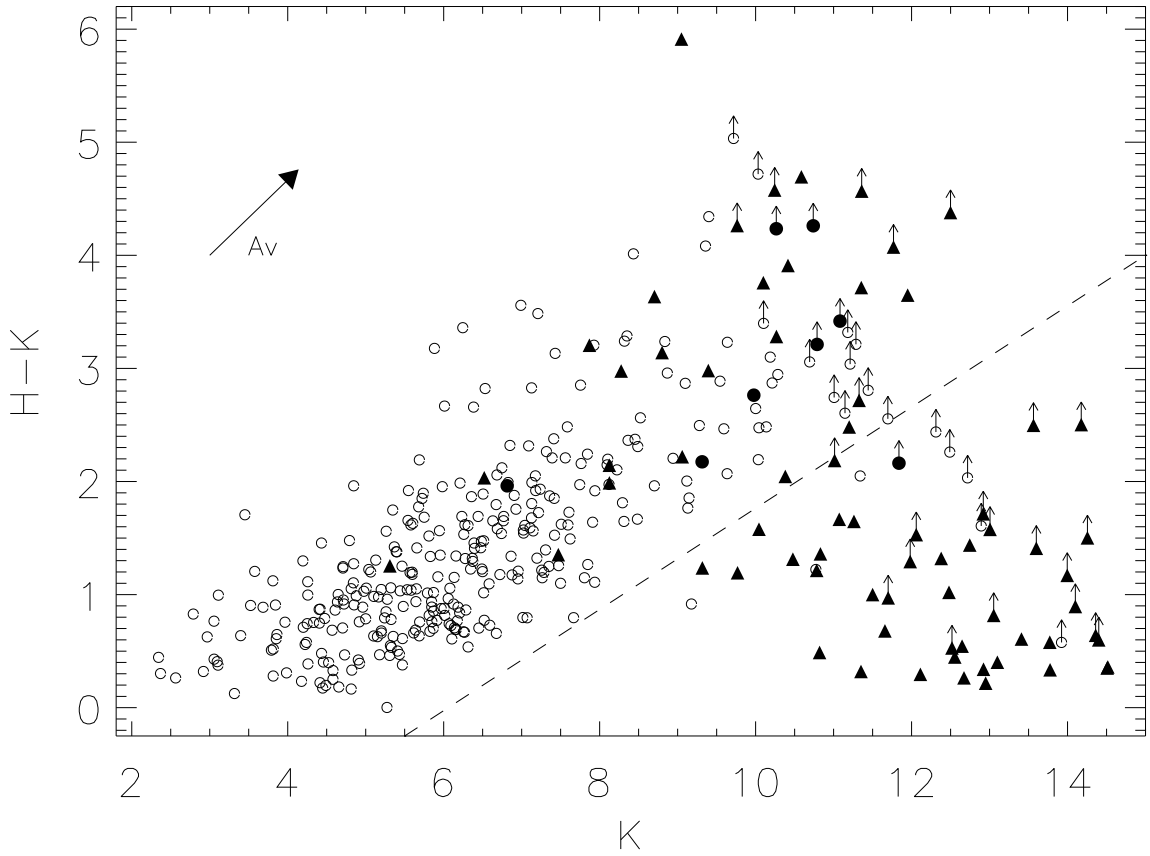

Fig. 2. H–K vs. K magnitude diagram of all 2MASS candidate counterparts of the 'GLMP sample' (filled triangles). The position of the OH/IR stars in the 'Arecibo sample' is also shown for comparison (open circles). Filled circles mark objects in common and H–K lower limits are represented by vertical arrows. The dashed line separates the counterparts with blue H–K colours suspected to be contaminated by field stars. The reddening vector corresponds to $A_V = 10^m$.

OH/IR stars with red IRAS colours ([12]–[25] > 0.5) and blue near-infrared colours (H–K < 1) are not expected to be variable OH/IR stars, but to be candidate post-AGB stars instead. The 'GLMP sample', however, was selected imposing that all sources must have a high IRAS variability index (VAR > 50), which should exclude post-AGB stars from the sample. We therefore rejected all 16 2MASS candidate counterparts with H–K < 1.0 because of being most likely reddened field stars.

Finally, it remains to consider the 11 2MASS candidate counterparts with $1.0 \leq$ H–K < 1.5. The probability for misidentification with a field star is 4% in this colour range. From the GLMP sources with MSX counterpart (N = 10) we expect therefor N ≈ 3 misidentified counterparts in this colour range, while 10 were actually found. Two of them with K < 8 follow the general correlation shown by the 'Arecibo sample', leaving ≈ 6 counterparts which cannot be explained as chance coincidences with field stars.

The possible nature of the sources from the 'blue subsample' will be discussed further in Section 4. Observations to detect variability in these counterparts are required to confirm the identifications.

3.3. Consistency checks

We made several consistency checks involving correlations between IRAS, MSX and 2MASS positions to validate the reliability of the MSX and 2MASS counterparts. In Table 2 we list the median and the mean separation (in arcsec) in Right Ascension (α) and Declination (δ) between 2MASS coordinates and the IRAS and MSX ones, together with the associated standard deviations. The median angular separation between the 2MASS and MSX positions is 1.3″, which is similar to the median separation of 1.7″ for the Arecibo sources found in Paper I.

In Fig. 4, we have plotted the angular separation distribution between 2MASS and MSX coordinates. Overplotted is the distribution of the blue 2MASS counterparts (H–K<1.0) which were considered to be field stars. Their angular separations are

Table 2. Median and mean separation (and standard deviation) between 2MASS and IRAS coordinates and between 2MASS and MSX coordinates.

	N	$\Delta\alpha$ median	$\Delta\alpha$ ($\sigma_{\Delta\alpha}$) mean	$\Delta\delta$ median	$\Delta\delta$ ($\sigma_{\Delta\delta}$) mean
2MASS–IRAS	59	3.8″	7.6″ (8.7″)	1.7″	2.0″ (2.4″)
2MASS–MSX	49	0.9″	1.2″ (1.1″)	1.0″	1.4″ (1.3″)

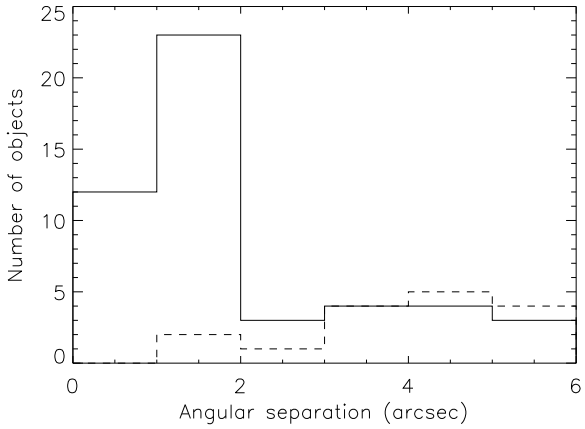

Fig. 4. Angular separation between 2MASS and MSX coordinates for the 49 objects in common (solid line). Angular separation between 2MASS and MSX coordinates for the 16 blue 2MASS counterparts considered to be field stars (dashed line)

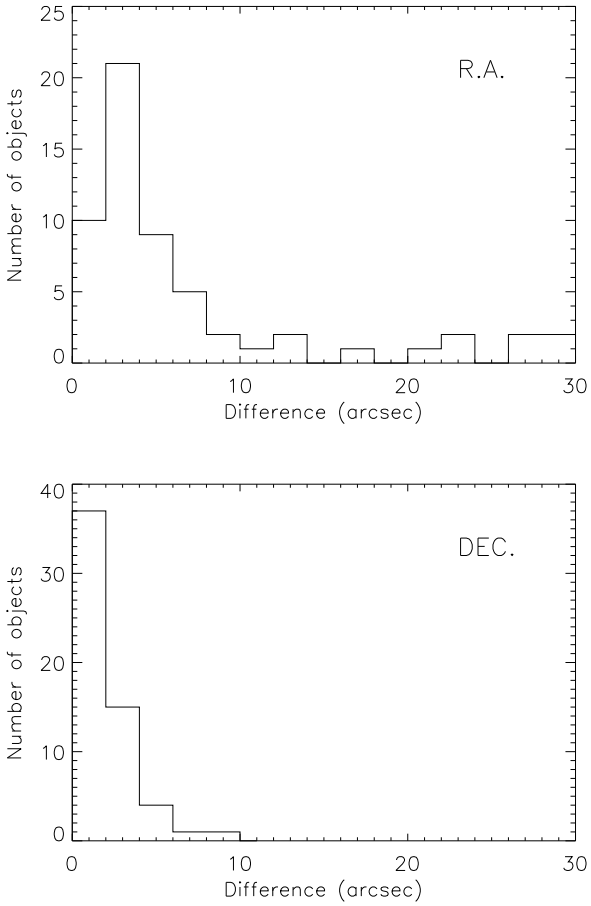

Fig. 5. Angular separation in right ascension (upper panel) and declination (lower panel) between 2MASS and IRAS coordinates for the 59 OH/IR stars for which a near-infrared counterpart was found. Not included in the R.A. distribution is one source with $|\Delta\alpha| = 41''$.

significantly larger, confirming their identification as probable field stars.

Much larger separations are found between 2MASS and the original IRAS coordinates. Figure 5 shows the distribution of these separations. While in declination they are within 6″ with just two exceptions, in right ascension we find a considerable number of objects showing separations larger than 10″. Similar separations have been found in Paper I for the Arecibo sources.

Given the positional uncertainties of the IRAS-PSC of up to 1′ (Paper I), counterparts with large 2MASS-IRAS separations might be misidentifications, if MSX coordinates are not available. Nine sources with rather large 2MASS-IRAS separations in RA ($\geq 20''$) are listed in Table 3. All of them but IRAS 18298–2111 have MSX counterparts. IRAS 18298–2111 is a bright IRAS source and its near-infrared counterpart has one of the reddest colours (H–K = 4.69) in our sample. Moreover, this source is located at galactic latitude $|b| = 5.6°$, where confusion is unlikely. We conclude therefore that the identification of this counterpart is correct.

3.4. The final set of 2MASS counterparts

We ended with 59 IRAS sources having a 2MASS counterpart, 49 coming from the subset of sources with an MSX counterpart. As tentative identifications we consider the 9 counterparts with $1.0 \leq$ H–K < 1.5 located outside H–K vs. K distribution of the Arecibo sources, and the counterparts detected only in the K-band and with a lower limit of H–K < 1.5, because the H–K constraint could not be determined. The same applies for IRAS 14562–5637, IRAS 17004–4119, IRAS 17276–2846 and IRAS 17392-3020, whose photometry is affected by blending problems, and for IRAS 17495–2534, which was just barely detected both in the K and H filters. Detection of variability is also required in these cases to confirm the counterpart.

Thus, the identification strategy provided in 36 cases a plausible near-infrared counterpart, while in 23 cases only a tentative near-infrared counterpart is provided. These 59 sources are listed in Table 3. The Table includes the IRAS name, the astrometric position from the 2MASS-PSC, the difference to the positions provided originally by IRAS and with the ones derived from the MSX6C, and the MSX name, when available.

Table 3. 2MASS and MSX counterparts of oxygen-rich AGB stars in the 'GLMP sample'.

GLMP	IRAS	2MASS Coordinates (J2000)		IRAS–2MASS $\Delta\alpha$ [″]	IRAS–2MASS $\Delta\delta$ [″]	IRAS–MSX $\Delta\alpha$ [″]	IRAS–MSX $\Delta\delta$ [″]	MSX6C_G	Opt
228	08425−5116 *	08 44 04.36	−51 27 41.9	3	0	2	−1	269.4419−05.4504	
309	11438−6330	11 46 14.00	−63 47 14.2	−2	2	−2	3	295.8065−01.8214	
320	12158−6443 *	12 18 35.48	−65 00 14.2	2	−3	3	−3	299.4688−02.3533	
333	12358−6323	12 38 48.35	−63 39 39.4	−1	1	0	0	301.5309−00.8231	
382	14247−6148	14 28 30.73	−62 01 35.7	0	0	3	0	314.0494−01.2684	
398	14562−5637 *	15 00 02.39	−56 49 44.2	6	−3	7	−2	319.8669+01.7534	
430	15471−4634	15 50 40.33	−46 43 16.9	2	−1	−2	−3	331.9853+05.7905	
435	15514−5323	15 55 21.13	−53 32 44.6	−26	8	−22	10	328.2246+00.0418	
447	16040−4708 *	16 07 39.47	−47 16 26.3	3	−2	3	−2	333.8253+03.4834	
463	16219−4823	16 25 41.89	−48 30 33.9	−1	0	0	−1	335.1416+00.4939	
503	16582−3059	17 01 29.83	−31 04 19.0	−6	0				
508	17004−4119 *	17 03 55.97	−41 24 00.8	1	2	−2	0	344.9293+00.0136	**
517	17030−3053	17 06 14.07	−30 57 38.3	−2	0	−3	2	353.5472+05.9448	
532	17107−3330	17 14 05.06	−33 33 58.0	−2	−1	−4	−2	352.4216+03.0672	
541	17151−3642 *	17 18 29.74	−36 46 07.2	−5	5	−4	0	350.3340+00.4777	
548	17171−2955	17 20 20.25	−29 58 22.8	−3	1	−3	−1	356.1310+04.0515	**
564	17242−3859 *	17 27 38.65	−39 02 10.1	12	−2	12	−1	349.4829−02.2940	**
573	17276−2846 *	17 30 48.35	−28 49 01.7	3	1	5	−2	358.3668+02.8054	
582	17316−3523	17 34 57.50	−35 25 52.6	6	0	6	1	353.2979−01.5367	
583	17317−3331	17 35 02.72	−33 33 29.4	−7	−1	−5	0	354.8833−00.5384	
589	17341−3529	17 37 30.29	−35 31 04.7	−17	3	−17	4	353.5039−02.0204	
594	17350−2413	17 38 08.85	−24 14 49.3	−2	0	−3	0	003.1080+03.8899	**
595	17351−3429 *	17 38 26.29	−34 30 41.0	−2	−1	−4	−2	354.4579−01.6437	
604	17367−3633 *	17 40 07.63	−36 34 41.4	−4	−3	−2	−2	352.8880−03.0333	
619	17392−3020 *	17 42 30.81	−30 22 07.3	−22	−2	−17	0	358.4249−00.1744	
626	17417−1630	17 44 39.87	−16 31 42.1	−4	−2				
636	17428−2438 *	17 45 56.97	−24 39 57.8	−2	−2	−3	−2	003.6854+02.1592	
649	17467−4256	17 50 20.50	−42 57 18.5	−3	−1				
656	17495−2534 *	17 52 39.59	−25 34 39.5	0	0	0	−2	003.6848+00.3883	
659	17504−3312	17 53 50.24	−33 13 26.3	−41	2	−41	0	357.2197−03.7085	
672	17545−3317	17 57 49.20	−33 17 47.6	1	−1	0	−2	357.5737−04.4663	
685	17577−1519	18 00 36.12	−15 19 44.6	−13	−2	−15	−2	013.4930+03.9153	
691	17583−3346	18 01 39.27	−33 46 00.5	−5	−1				**
704	18006−1734 *	18 03 36.86	−17 34 00.4	−4	−1	−4	−1	011.8974+02.1862	
709	18015−1608	18 04 28.28	−16 07 52.3	−8	0	−10	0	013.2508+02.7102	
727	18081−0338 *	18 10 49.48	−03 38 14.2	−6	0				
731	18091−0855 *	18 11 56.55	−08 54 46.1	−4	−3	−3	−3	020.4676+04.5958	**
730	18091−2437 *	18 12 16.13	−24 36 42.9	−6	−2	−5	−1	006.7152−02.9972	
743	18107−0710	18 13 30.01	−07 09 48.2	−3	−1	−4	−2	022.1975+05.0855	
755	18152−0919 *	18 17 58.57	−09 18 31.5	−20	−1	−21	−1	020.8254+03.0967	
756	18182−1504 *	18 21 06.83	−15 03 20.0	−12	−4	−13	−2	016.1169−00.2903	
760	18187−0208 *	18 21 18.76	−02 07 01.1	−4	−2	−3	−4	027.5923+05.7240	
767	18201−2549	18 23 12.28	−25 47 58.7	−1	2				
768	18211−1712	18 24 05.54	−17 11 11.9	−6	−1	−7	−1	014.5704−01.9215	
784	18257−1052	18 28 30.97	−10 50 48.5	3	−6	4	−2	021.4566+00.4911	
786	18262−0735	18 28 59.86	−07 33 23.0	−5	−2	−6	−3	023.6510+01.5062	
787	18266−1239	18 29 28.74	−12 37 53.1	8	1	9	3	019.2086−00.9527	**
791	18277−1059	18 30 30.92	−10 57 33.4	28	1	29	1	020.8085−00.4024	
793	18298−2111	18 32 48.56	−21 09 37.6	28	1				
794	18299−1705	18 32 50.75	−17 02 48.5	−4	0	−4	−1	015.6638−03.7108	**
799	18310−2834	18 34 13.78	−28 32 21.6	−2	−2				
810	18361−0647	18 38 50.54	−06 44 49.6	−32	14	−34	14	025.4948−00.2879	
826	18432−0149 *	18 45 52.40	−01 46 42.5	6	0	6	0	030.7147+00.4264	
831	18460−0254	18 48 41.97	−02 50 25.4	−23	−10	−24	−6	030.0908−00.6866	
835	18475−1428	18 50 22.90	−14 24 30.7	−6	−3				
839	18488−0107 *	18 51 26.02	−01 03 56.0	−3	2	−6	−2	031.9844−00.4849	
878	19069+1335	19 09 16.61	+13 40 27.9	−6	−3	−6	−3	047.1168+02.3242	
884	19087+1006 *	19 11 10.00	+10 11 43.7	−30	−14	−28	−8	044.2404+00.3090	
892	19122−0230	19 14 54.84	−02 25 28.8	−7	−2				

Note: * tentative 2MASS identification; ** shows optical counterpart

The objects with tentative identification have been labeled with an asterisk.

All the objects without an identified 2MASS counterpart but with an MSX one are given in Table 4. This Table includes the IRAS name, the MSX coordinates, the difference to the original IRAS coordinates and the associated MSX object name. Only IRAS 18479–2514 and IRAS 18195-2804 had neither an MSX nor 2MASS counterpart. For these two sources no improvement to the IRAS coordinates was possible. Their IRAS coordinates have also been tabulated in Table 4.

In Table 5 we present the J, H and K near-infrared 2MASS magnitudes (or lower limits) for the 59 sources with a plausible or tentative near-infrared identification. The lower limits have been obtained from nearby stars with similar or even greater brightnesses. For the 5 objects which have been identified only on the 2MASS images, but have no associated entry in the 2MASS-PSC, we have obtained their photometry directly from the 2MASS images, with the exception of IRAS 17495–2534 because it was strongly blended. We have also measured the photometry in the K band for IRAS 17171–2955, as the 2MASS-PSC only provides a lower limit.

3.5. Search for optical counterparts

In order to search for the optical counterparts of those GLMP sources for which we found a near-infrared counterpart, we inspected their positions on the optical images extracted from the DSS2 (Djorgovski et al. 2001) in the red filter, which covers the spectral range 6 000 – 7 000 Å with a maximum efficiency around 6 700 Å. We used a $1'' \times 1''$ box centered on the nominal 2MASS source position.

The majority (91%) of the objects did not show any optical counterpart, and only 8 objects had a faint optical counterpart. Based on our expectation that the sources in the 'GLMP sample' would have optically thick CSE the association with optically visible counterparts is questionable. However, also in the 'Arecibo sample' restricted to the same IRAS colour range ($F_\nu(12\mu m)/F_\nu(25\mu m) \leq 0.50$) a similar rate of 90% was found without the optical counterpart. The identified counterparts could be either real and possibly observed close to maximum light, or misidentifications with reddened field stars. Variability studies of the optical counterparts would help with their confirmation. The objects with an optical counterpart have been labeled in Table 3.

3.6. The atlas of optical and near-infrared counterparts

The results of the identifications are displayed as an atlas of finding charts. An example of the atlas images is given in Fig. 6. For each source of the 'GLMP sample' a chart was put together as a mosaic of 4 images containing the optical image taken from the DSS2 in the upper left panel, and the J, H and K images from the 2MASS in the upper right, lower left and lower right panels, respectively. The size of the field shown in each band is $4.6' \times 4.6'$. For each source we marked the position of the proposed optical/near infrared counterpart with a circle in each of the available frames. In those cases where an optical/near-infrared counterpart was not found the circle was drawn at the position where the source should be located according to the best astrometric coordinates available (IRAS or MSX). The complete atlas can be accessed electronically at: http://www.edpsciences.org

4. Near-infrared properties

4.1. Near-infrared brightness distribution

The typical near-infrared counterpart of objects from the 'GLMP sample' is very red (H–K>2). 75% of the GLMP sources were not detected in the J-band, 66% were not detected in the H band, and 37% were not detected even in the K band.

Figure 7 shows the J, H and K magnitude distribution of all the GLMP sources with near-infrared counterparts and photometric measurements in at least one band. Most of the sources observed have faint near-infrared counterparts with the magnitude distribution peaking at $\approx 10^m$ in K, $\approx 12^m$ in H and $\geq 14^m$ in J. The distributions are not strongly peaked and are clearly limited by the 2MASS sensitivity limit, especially in the J band.

As it was discussed in Paper I for the sources in the 'Arecibo sample', the observed magnitude distribution can in principle be attributed to three main reasons:

i) the different intrinsic luminosity of the sources in the sample,

ii) the different apparent brightness expected from sources located at a wide range of distances, and

iii) the differences in optical thickness of the CSEs.

Compared to the magnitude distribution of the 'Arecibo sample' (Figure 5 of Paper I) peaking at $\approx 6^m$ in K, $\approx 6.5^m$ in H and $\geq 7.5^m$ in J, the mean near-infrared brightness of the 'GLMP sample' is several magnitudes fainter. The sources in the 'GLMP sample' are not expected to be intrinsically less luminous than the ones in the 'Arecibo sample' (actually we would expect the contrary, since they are suspected to represent a higher mass population). Thus, unless the sources in the 'GLMP sample' are preferentially found at larger distances than those in the 'Arecibo sample', the most probable explanation for the systematic fainter brightnesses are the greater optical thickness of their CSEs, in comparison with the optically thinner shells of the bluer Arecibo sources.

4.2. Near infrared colours

The near-infrared colours of the 'GLMP sample' are shown as a J−H vs. H−K colour-colour diagram in Figure 8. Included are all sources belonging to both the 'red subsample' (filled triangles) and the 'blue subsample' (filled squares) with at least data available in the H and K bands. For objects not detected in J, lower limits for the J−H colours were calculated and these are indicated by horizontal arrows. The objects with deblending problems have not been included. For comparison, we have also plotted the colours of the sources in the 'Arecibo sample'.

In general, the 'GLMP sample' follows the correlation shown by the more standard OH/IR stars of the 'Arecibo sample', although the two subsamples are also clearly separated

Table 4. MSX counterparts of oxygen-rich AGB stars in the 'GLMP sample', without near-infrared counterparts identified.

GLMP	IRAS	MSX Coordinates (J2000)		IRAS−MSX $\Delta\alpha$ [″]	IRAS−MSX $\Delta\delta$ [″]	MSX6C_G
239	09024−5019	09 04 03.3	−50 31 32	0	4	270.7424−02.4384
410	15198−5625	15 23 42.7	−56 36 08	1	1	322.7729+00.2860
418	15327−5400	15 36 35.9	−54 10 29	−5	1	325.6578+01.2432
465	16236−5332	16 27 39.3	−53 39 04	−13	2	331.6587−03.3024
519	17055−3753	17 08 57.3	−37 56 50	6	0	348.2670+01.3225
536	17128−3528	17 16 12.9	−35 32 12	−1	0	351.0725+01.5639
555	17207−3632	17 24 07.4	−36 35 39	5	−3	351.1189−00.3517
566	17251−2821	17 28 18.5	−28 23 57	3	−4	358.4140+03.4923
577	17292−2727	17 32 23.4	−27 29 58	4	−3	359.6629+03.2315
585	17323−2424	17 35 26.0	−24 26 32	−6	2	002.6111+04.3084
602	17361−2358	17 39 15.0	−23 59 55	3	−3	003.4525+03.8089
603	17367−2722	17 39 52.4	−27 23 32	−4	−4	000.6467+01.8893
605	17368−3515	17 40 12.9	−35 16 41	2	−3	354.0019−02.3600
624	17411−3154	17 44 24.0	−31 55 40	−17	1	357.3108−01.3371
629	17418−2713	17 44 58.8	−27 14 43	−1	−2	001.3690+01.0025
664	17521−2938	17 55 21.8	−29 39 13	0	1	000.4720−02.1918
673	17545−3056	17 57 48.4	−30 56 25	0	−2	359.6212−03.2926
692	17584−3147	18 01 41.8	−31 47 56	−4	−2	359.2842−04.4385
699	18000−2835	18 03 13.0	−28 35 43	−29	2	002.2442-03.1547
705	18007−1841	18 03 39.0	−18 41 10	21	4	010.9257+01.6294
712	18019−3121	18 05 12.1	−31 21 45	−1	2	000.0313−04.8783
717	18040−2726	18 07 09.0	−27 25 52	−5	−4	003.6860−03.3459
718	18040−2953	18 07 18.3	−29 53 10	−9	−3	001.5478−04.5617
732	18092−2347	18 12 20.5	−23 46 57	−17	−3	007.4526−02.6149
733	18092−2508	18 12 21.9	−25 07 21	−4	−1	006.2765−03.2604
740	18100−1915	18 13 03.2	−19 14 19	−6	−1	011.5218−00.5826
763	18195−2804 *	18 22 40.2	−28 03 08			
765	18198−1249	18 22 43.1	−12 47 42	−12	−2	018.2955+00.4291
783	18257−1000	18 28 31.0	−09 58 15	−35	−3	020.6796+00.0841
788	18268−1117	18 29 35.6	−11 15 54	3	0	020.4328−00.3439
811	18361−0036	18 38 45.1	−00 33 22	2	1	030.9892+02.5686
837	18479−2514 *	18 51 00.9	−25 11 06			
843	18518+0558	18 54 17.4	+06 02 34	−1	−2	038.6366+02.1198
888	19112+1220	19 13 37.4	+12 25 38	−16	−8	046.4992+00.8092
916	19254+1724	19 27 41.1	+17 30 36	1	−1	052.5814+00.2014

Note: * IRAS coordinates.

in this diagram. The distribution of the 'red subsample' is restricted at the red end by the limited sensitivity of 2MASS, especially in the J band. Extrapolating the correlation between the colours, the reddest object (IRAS 11438–6330) with H–K = 5.91 should have an expected colour J–H ≈ 8 well beyond the limit of J−H ≈ 4.5 following from Figure 8.

In Paper I we have shown that on average the redder an object is in the far-infrared, the redder is its near-infrared counterpart (see Figure 8 of Paper I). The Arecibo sources with IRAS colours satisfying the selection criteria imposed for the 'GLMP sample' (filled circles in Fig. 8) are all located in the red part of the near-infrared colour-colour distribution. Actually, the near-infrared colours of the GLMP sources overlap with the red end of the Arecibo J−H vs. H−K colour-colour distribution. There are two outliers: IRAS 18299 – 1705, which is discussed below, and IRAS 17171–2955, with H–K ≈ 2.5 and J–H ≈ 1.0. The 2MASS photometry of this source in the J- and H-band is however biased by a nearby star that probably has contaminated the background estimation. This makes its near-infrared colours unreliable. Except for IRAS 18299 – 1705, the near-infrared colours of the 'red subsample' therefore corroborate the results obtained from the 'Arecibo sample' that the objects with optically thicker CSEs reveal themselves in the far-infrared as well as in the near-infrared by their redder colours.

4.3. *IRAS* 18299 – 1705*: a post-AGB candidate?*

IRAS 18299 – 1705 (J–H ≈ 1.7; H–K ≈ 1.3; K=5.31) is located to the left of the dividing line in Figure 2 and is therefore part of the 'red subsample'. However, in the J−H vs. H−K diagram it has very blue colours, different from the rest of the 'red subsample', and it has the brightest near-infrared counterpart of the 'GLMP sample'. Instead of the typical double-peaked maser profile of regular OH/IR stars, this source shows a single peak

Table 5. 2MASS JHK band photometry of the oxygen-rich AGB stars of the 'GLMP sample'

IRAS	2MASS photometry [mag]		
	J	H	K
08425−5116	13.79 ± 0.03	12.19 ± 0.03	10.83 ± 0.02
11438−6330	> 17 ———	14.96 ± 0.09	9.05 ± 0.02
12158−6443	12.77 ± 0.02	10.96 ± 0.02	9.77 ± 0.02
12358−6323	> 14 ———	> 13 ———	12.06 ± 0.04
14247−6148	13.34 ± 0.03	10.27 ± 0.02	8.12 ± 0.02
14562−5637	15.20 ± 0.07	* 13.73 ———	* 13.20 ———
15471−4634	> 16 ———	15.60 ± 0.16	11.95 ± 0.03
15514−5323	15.11 ± 0.04	11.62 ± 0.03	10.04 ± 0.02
16040−4708	15.87 ± 0.09	14.18 ± 0.09	12.75 ± 0.04
16219−4823	> 15 ——-	> 14 ———	11.33 ± 0.04
16582−3059	> 17 ———	> 16 ———	13.56 ± 0.05
17004−4119	15.89 ± 0.10	13.23 ± 0.05	* 11.52 ———
17030−3053	> 17 ———	> 16 ———	12.50 ± 0.03
17107−3330	> 16 ———	13.86 ± 0.05	10.10 ± 0.03
17151−3642	> 13 ———	** 12.5 ± 0.5	** 11.5 ± 0.5
17171−2955	14.71 ± 0.08	13.68 ± 0.09	** 11.2 ± 0.1
17242−3859	> 13 ———	> 12 ———	11.70 ± 0.04
17276−2846	10.89 ± 0.04	* 9.47 ———	* 8.79 ———
17316−3523	> 16 ———	> 14 ———	13.01 ± 0.06
17317−3331	> 16 ———	> 14 ———	10.24 ± 0.03
17341−3529	14.62 ± 0.06	11.28 ± 0.03	9.06 ± 0.02
17350−2413	> 14 ———	> 13 ———	11.01 ± 0.03
17351−3429	> 14 ———	> 13 ———	11.98 ± 0.04
17367−3633	> 14 ———	> 13 ———	12.52 ± 0.03
17392−3020	14.02 ± 0.06	11.60 ± 0.05	* 9.12 ———
17417−1630	> 17 ———	14.32 ± 0.04	10.41 ± 0.02
17428−2438	> 15 ———	> 15 ———	** 14.4 ± 0.2
17467−4256	> 17 ———	15.07 ± 0.08	11.35 ± 0.02
17495−2534	> 13 ———	> 12 ———	> 11 ———
17504−3312	> 15 ———	12.91 ± 0.02	11.26 ± 0.02
17545−3317	> 15 ———	> 14 ———	12.92 ± 0.07
17577−1519	14.41 ± 0.05	12.43 ± 0.03	10.38 ± 0.02
17583−3346	> 15 ———	13.55 ± 0.05	10.27 ± 0.02
18006−1734	13.30 ± 0.04	11.79 ± 0.03	10.48 ± 0.03
18015−1608	> 14 ———	12.38 ± 0.04	9.39 ± 0.02
18081−0338	12.41 ± 0.03	10.55 ± 0.03	9.32 ± 0.02
18091−0855	14.37 ± 0.04	13.50 ± 0.04	12.48 ± 0.03
18091−2437	> 15 ———	> 15 ———	** 14.36 ± 0.08
18107−0710	15.60 ± 0.08	11.07 ± 0.03	7.87 ± 0.02
18152−0919	> 16 ———	> 15 ———	14.00 ± 0.08
18182−1504	> 15 ———	** 13.70 ± 0.07	** 12.38 ± 0.04
18187−0208	13.61 ± 0.03	12.00 ± 0.02	10.78 ± 0.02
18201−2549	15.39 ± 0.06	11.25 ± 0.03	8.28 ± 0.02
18211−1712	> 12 ———	11.94 ± 0.11	8.80 ± 0.09
18257−1052	11.70 ± 0.03	8.82 ± 0.04	7.47 ± 0.03
18262−0735	> 16 ———	12.34 ± 0.03	8.70 ± 0.02
18266−1239	14.05 ± 0.02	12.74 ± 0.03	11.07 ± 0.02
18277−1059	> 16 ———	> 14 ———	9.76 ± 0.03
18298−2111	> 16 ———	15.28 ± 0.09	10.59 ± 0.02
18299−1705	8.23 ± 0.02	6.56 ± 0.03	5.31 ± 0.02
18310−2834	> 16 ———	> 15 ———	11.77 ± 0.03
18361−0647	> 16 ———	> 15 ———	11.36 ± 0.03
18432−0149	> 16 ———	> 15 ———	13.60 ± 0.05
18460−0254	> 17 ———	> 15 ———	14.26 ± 0.09
18475−1428	11.52 ± 0.02	8.55 ± 0.04	6.52 ± 0.02
18488−0107	> 16 ———	> 13 ———	13.05 ± 0.06
19069+1335	> 17 ———	> 16 ———	14.18 ± 0.08
19087+1006	> 17 ———	> 15 ———	14.10 ± 0.08
19122−0230	12.94 ± 0.03	10.11 ± 0.03	8.12 ± 0.03

Note: * The accuracy of the photometry is affected by deblending problems acording to 2MASS catalogue; ** Photometry obtained from the 2MASS images.

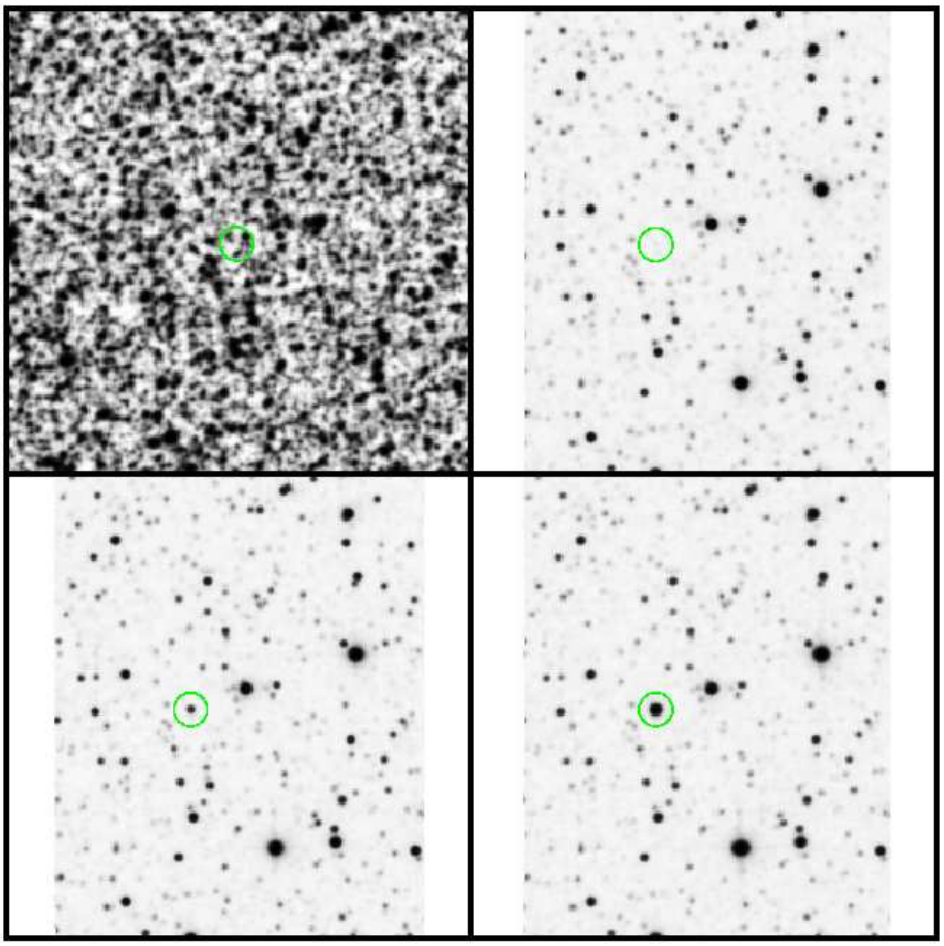

Fig. 6. Atlas images for IRAS 18201–2549. The upper panel shows the optical DSS2 R band (left) and the 2MASS J band (right) images, and the lower panel shows the H-band (left) and K-band (right) images. The adopted counterpart is indicated by a circle.

1612 MHz OH maser (te Lintel Hekkert 1991). Its LRS spectrum does not show the very strong 9.7μm absorption feature characteristic of optically thick CSEs, but a red continuum with either a weak 9.7μm absorption feature or the 11.3μm PAH feature in emission (Kwok et al. 1997). This source is therefore peculiar.

Lewis et al. (2004) analysed the 2MASS counterparts of a third of the 'Arecibo sample' of OH/IR stars. They claimed that most of the Arecibo sources with red far-infrared ([12]–[25] $\gtrsim$ 0.0) colour presented blue near-infrared colours in the J–K vs. H–K diagram, similar to those of our 'blue subsample'. They interpreted these colours as the result of a drastic decrease of the mass-loss rates from the central star leading to a decrease of the dust opacity in the near environment of the central star. This allows the central star to reappear in the near-infrared and to dominate the colours. Since these objects have strongly decreased their mass-loss rate, the authors inferred that these objects have detached shells.

IRAS 18299 – 1705 is a good case for an AGB star with a detached shell, and may have developed into the post-AGB phase. It is however a single case in our sample, and we are therefore not able to confirm the high incidence of detached shells among the AGB stars with very red IRAS colours, as suggested by Lewis et al. (2004). Photometric monitoring is required to confirm the variability of IRAS 18299 – 1705 inferred by the IRAS variability index (VAR=74), which may contradict its post-AGB classifcation.

4.4. The nature of the blue counterpart candidates

The 'blue subsample' is outstanding in the H–K vs. K (Fig. 2) as well as in the J−H vs. H−K diagram (Fig. 8). Their blue near-infrared colours are incompatible with the high optical thickness of their CSEs as inferred from their IRAS colours. The only sources showing red far-infrared colours and blue near-infrared colours are post-AGB stars, e.g. stars with a detached shell. As post-AGB stars are no longer variable, or at most with small amplitudes (Kwok 1993), we did not expect them to be part of the 'GLMP sample'.

The case of IRAS 18299 – 1705 shows however that the IRAS variability index might not be a reliable selection criterion to reject post-AGB stars. There might be more of them among our 'blue subsample'. The counterparts from the 'blue subsample' differ however from IRAS 18299 – 1705 by their

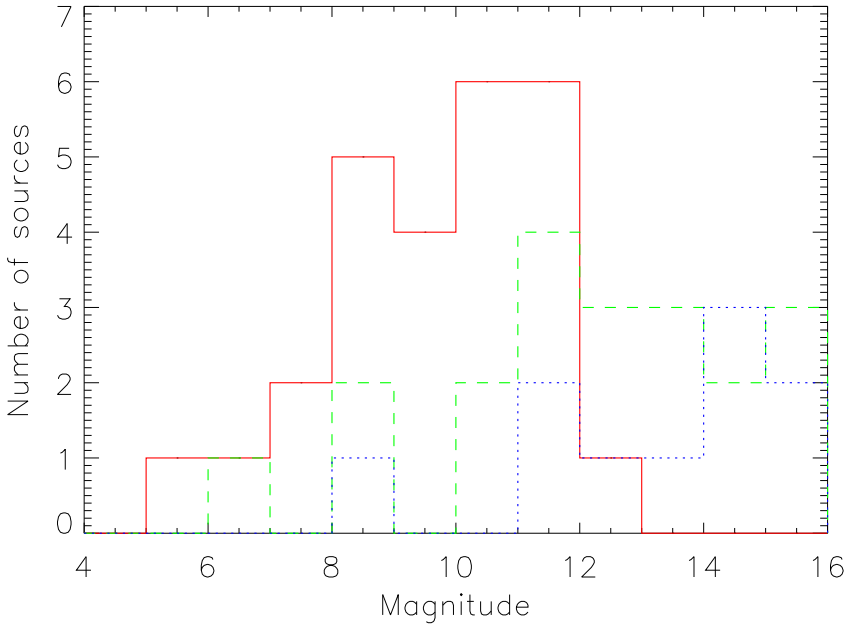

Fig. 7. J-band (*dotted line*), H-band (*dashed line*), and K band (*solid line*) magnitude distribution of the sources included in the 'GLMP sample'.

faintness (K>9 mag), and because of the higher surface density of faint infrared sources they might be simply misidentified field stars. Counterpart candidates with H–K<1.0 were already rejected for this reason (see Section 3.2.2).

The case is less clear for the redder sources. Among the three Arecibo sources with near-infrared colours of the 'blue subsample' (see Fig. 2), two are known to have peculiarities. One is IRAS 18455+0448, for which Lewis (2002) found that the OH maser decreased continuously and finally disappeared over < 12 years. He argues that the mass-loss rate has dropped and that the star is now leaving the AGB. The other is IRAS 19319+2214, which shows a peculiar OH maser profile with several peaks (Lewis et al. 2004). In this case the star may have several OH masing shells expanding with different velocities. Among the 'blue subsample' is also the well known variable OH/IR star OH 19.2–1.0 (IRAS 18266–1239; J–H ≈ 1.3; H–K ≈ 1.7), showing a multiple-peak OH spectrum, which has been explained by a bipolar structure of the CSE (Chapman 1988). The peculiarities of the OH masers in these three stars may indicate that their mass-loss process (e.g. mass-loss rate or geometry of the outflow) is currently experiencing fast changes, which might be responsible for the relatively blue colours of their near-infrared counterparts. The three cases show that the faint counterparts with H–K > 1 cannot be all misidentifications. Instead, the deviating near-infrared colours may point to AGB stars in which the mass loss rates have recently varied drastically over time intervals comparable to the dynamical time scale of their shells.

We conclude therefore that the nine remaining objects from the 'blue subsample' are a mixture of misidentifications and peculiar AGB stars, requiring confirmation of their near-infrared counterparts by further observations.

4.5. Near- and far-infrared properties

A way to visualize the near- and far-infrared properties of the sources in the GLMP sample is to study their distribution in the K−[12] vs. [12]−[25] colour-colour diagram (Figure 9). In the blue part of the distribution the K−[12] colour provides information on the relative contribution of the near-infrared emission, dominated by the central star and by the hot dust surrounding it, and of the far-infrared emission, mainly coming from the cool dust in the circumstellar shell, to the overall spectral energy distribution. In the red part the K−[12] colour is fully dominated by the outer cool CSE. As we have shown in Paper I, the correlation of the K−[12] with the IRAS [12]−[25] colour shown by the Arecibo OH/IR stars could be interpreted as an additional indicator of the optical thickness of the CSE for a given source. In Figure 9 we have plotted the GLMP OH/IR stars together with those of the 'Arecibo sample'. For those sources with no photometric measurement in K, upper limits were converted to lower limits in the K−[12] colour. K−[12] colour was taken as $-2.5 \log \frac{F_\nu(K)}{F_\nu(12)}$, adopting a zero-magnitude flux in the K-band of 667 Jy (Cohen et al. 2003).

The scatter in Fig. 9 is mostly attributed to the expected strong variability of the sources and the non-contemporaneous near- and far-infrared observations. The expected dispersion due to variability is indicated by the dashed lines (see Paper I). Variability is however not able to explain fully the scatter seen in Fig. 9. For example, at [12]−[25] ≈ 0.8 the range in

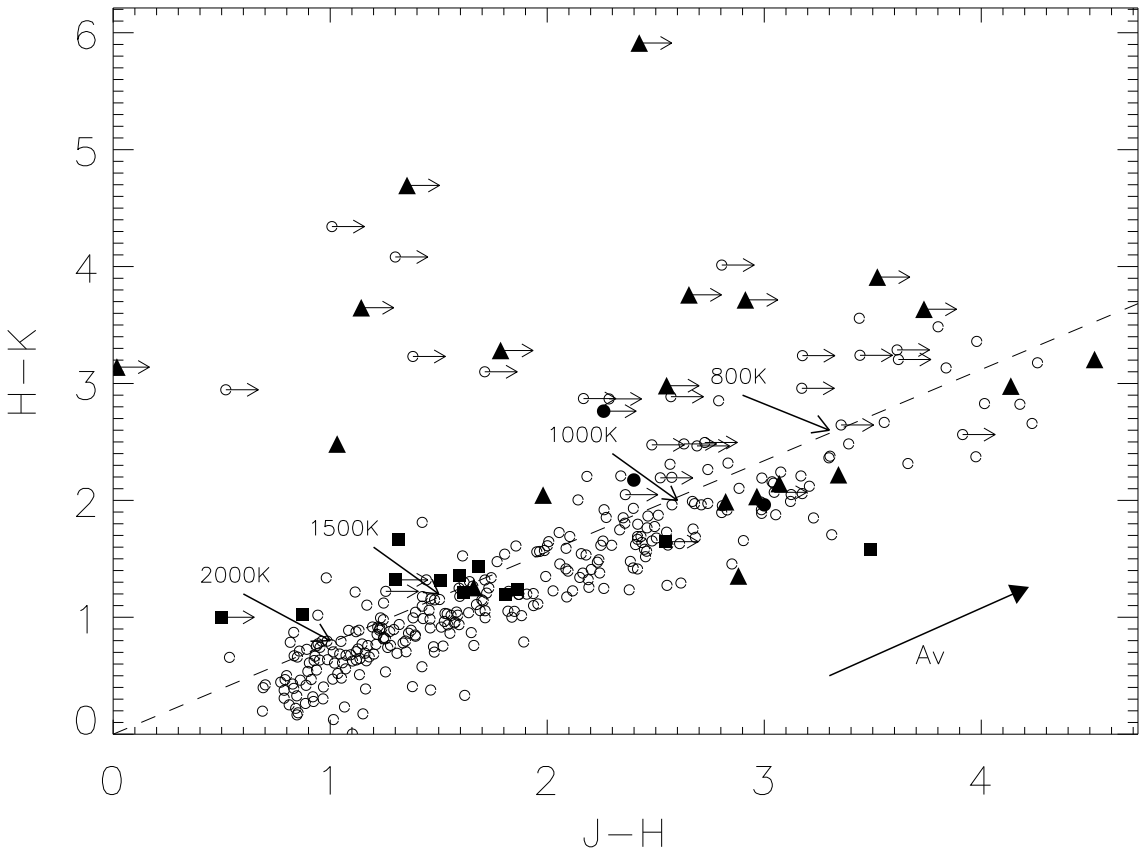

.

Fig. 8. Near-infrared J–H vs. H–K colour-colour diagram of the sources belonging to both the 'red subsample' (filled triangles) and the 'blue subsample' (filled squares) with H- and K-band detections (N = 32). For comparison, the near-infrared colours of the sources in the 'Arecibo sample' are also shown (open circles; filled circles for objects in common). J–H lower limits are indicated by horizontal arrows. The location of black-bodies of different temperatures and the reddening corresponding to $A_V = 10^m$ are also indicated.

K−[12] colour is ≈ 10 mag, which is approximately twice the range expected due to variability.

In general, the 'GLMP sample' of OH/IR stars confirms the colour trend shown by the 'Arecibo sample' of OH/IR stars. Using both samples we have fitted an exponential function to the observational data, weighting each data point according to the associated errors in each colour and omitting the lower limits. We obtained the following equation:

$$\mathrm{K}-[12] = 3.44\, e^{0.86([12]-[25])} - 1.74$$

This equation represents a parametrization of the colours of the 'O-rich AGB sequence', and has been plotted in Figure 9 with a solid line.

In general, the position of the GLMP OH/IR stars in the K−[12] vs. [12]−[25] colour-colour diagram is an extension toward redder colours of the sequence of colours associated with the Arecibo sources. The 'blue' and the 'red subsample' defined in the near-infrared cannot be distinguished in this diagram. The large scatter of the K−[12] colours inhibits its use as an identification criterion of near-infrared counterparts.

5. Conclusions

We have presented an atlas of optical/near-infrared finding charts and near-infrared photometric data for 94 OH/IR stars taken from the GLMP catalogue, considered to be an extension toward redder colours and thicker shells of the sources in the 'Arecibo sample'. For 59 sources we successfully identified their near-infrared counterparts in the 2MASS-PSC and determined new positions with an accuracy of ≈ 0.2″. The identifications were possible in many cases with the help of improved positional information taken from the MSX6C (accuracy ≈ 1.8″) as an intermediate step, and confirmed through the analysis of their near- and far-infrared colours. For about a third of the sample (N=34 sources) no near-infrared counterpart could be found even at 2.2μm. These stars most likely have the CSEs with the highest obscuration achieved by AGB stars.

As expected by the selection criteria, the near- and far-infrared properties of most of the identified GLMP sources are similar to those of the redder objects in the 'Arecibo sample' analyzed in Paper I. Some near-infrared counterparts showed

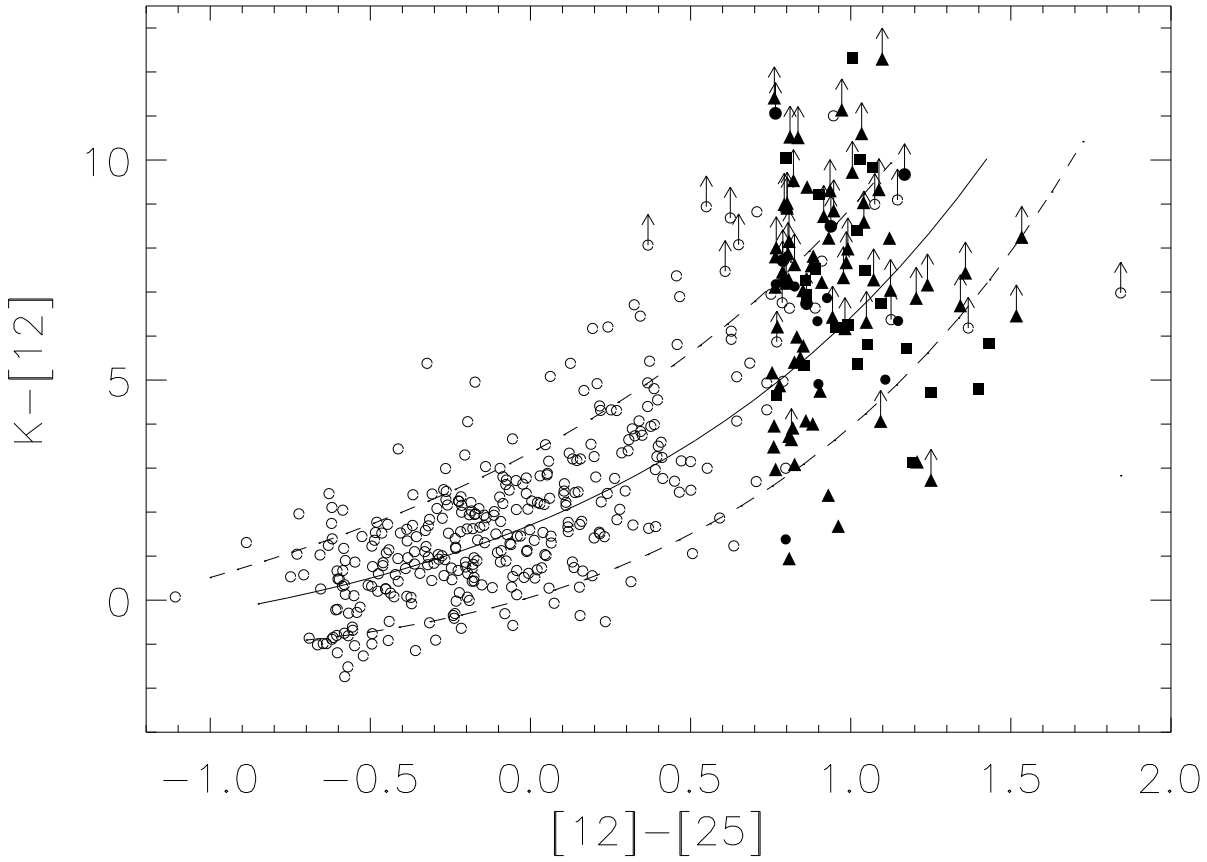

.

Fig. 9. K−[12] vs. [12]−[25] colour-colour diagram of all GLMP stars with K band photometry (filled triangles; filled squares for those belonging the 'blue subsample') together with those of the 'Arecibo sample' (open circles; filled circles for objects in common). Upper limits in K were converted to lower limits in K−[12] colour (arrows). The continuous line corresponds to the best fit to the observed data (see text). The dashed lines correspond to the dispersion expected from the variability of the sources in the K and at 12 μm band.

surprisingly blue colours. Among them is IRAS 18299 – 1705, which has also the brightest 2MASS counterpart. This source likely has a detached shell and might be a post-AGB star. The other counterparts with blue colours are a mixture of misidentifications with field stars and peculiar case, in which the blue colours might be due to a recent strong decrease of the mass loss rate leading to a corresponding decrease of the optical thickness of their circumstellar shells.

The high fraction of GLMP sources still unidentified in the near-infrared and the near- and far-infrared colours of the majority of the sources identified in the 2MASS confirm their classification as oxygen-rich AGB stars highly obscured by optically thick CSEs. They belong to the same population of heavily reddened AGB stars, as the reddest OH/IR stars in the 'Arecibo sample', although not in all of them has OH maser emission been detected yet.

The observational results presented here, together with those already included in Paper I, will be discussed in detail in a broader astrophysical context in a future paper of this series.

Acknowledgements. This work has been supported by the Spanish Ministerio de Ciencia y Tecnología through travel grants (AYA2003−09499). This research has made use of the SIMBAD database, operated at CDS, Strasbourg, France. We acknowledge also the use of the Digitized Sky Survey, based on photographic data obtained using the UK Schmidt Telescope. The UK Schmidt Telescope was operated by the Royal Observatory Edinburgh, with funding from the UK Science and Engineering Research Council, until 1988 June, and thereafter by the Anglo-Australian Observatory. Original plate material is copyright (c) of the Royal Observatory Edinburgh and the Anglo-Australian Observatory. The plates were processed into the present compressed digital form with their permission. The Digitized Sky Survey was produced at the Space Telescope Science Institute under US Government grant NAG W-2166. This publication makes also use of data products from the Two Micron All Sky Survey, which is a joint project of the University of Massachusetts and the Infrared Processing and Analysis Center/California Institute of Technology, funded by the National Aeronautics and Space Administration and the National Science Foundation.

References

Bedijn, P. J. 1987, A&A, 186, 136

Beichman, C. A., Neugebauer, G., Habing, J. H., Clegg, P., & Chester, T. J. 1988, *IRAS Catalogs and Atlases, Volumen 1: Explanatory Supplement*, US Government Printing Office, Washington, DC

Bowers, P. F., & Knapp, G. R. 1989, ApJ, 347, 325

Chapman, J. M. 1988, MNRAS, 230, 415

Chengalur J.N., Lewis, B.M., Eder, J., Terzian, Y. 1993, ApJS, 89, 189

Cohen, M., Wheaton, W. A., & Megeath, S. T. 2003, AJ, 126, 1090

Cohen, M., Parker, Q. A., Chapman, J. 2005, MNRAS, 357, 1189

Cutri, R. M., Skrutskie, M. F., van Dyk, S. et al. 2003, *2MASS All-Sky Catalog of Point Sources*

Djorgovski, S. G., Gal, R. R., de Carvalho, R. R., et al. 2001, 199th American Astronomical Society Meeting, BAAS, 33, 1461

Eder, J., Lewis, B.M., Terzian, Y. 1988, ApJSS, 66, 183

Egan, M. P., Price, S. D., & Kraemer, K. E. 2003, The Midcourse Space Experiment (MSX) Point Source Catalog Version 2.3

Engels, D., Kreysa, E., Schultz, G. V., & Sherwood, W. A. 1983, A&A, 124, 123

García-Lario, P. 1992, Ph.D. Thesis, Universidad de La Laguna, Tenerife (Spain)

García-Lario, P., Manchado, A., Pych, W., & Pottasch, S. R. 1997, A&AS, 126, 479

Gaylard, M. J., West, M. E., Whitelock, P. A., & Cohen, R. J. 1989, MNRAS, 236, 247

Harvey, P. M., Bechis, K. P., Wilson, W. J., & Ball, J. A. 1974, ApJS, 27, 331

Herman, J., Burger, J. H., & Penninx, W. H. 1986, A&A 167, 247

Hu, J. Y., Slijkhuis, S., de Jong, T., & Jiang, B. W. 1993, A&ASS, 100, 413

Jiménez-Esteban, F. M., Agudo-Mérida, L., Engels, D., & García-Lario, P. 2005a, A&A, 431, 779

Jiménez-Esteban, F. M., Engels, D., & García-Lario, P. 2005b, in preparation

Jiménez-Esteban, F. M., García-Lario, P. L., Manchado, A., & Engels, D. 2005c, in preparation

Kwok, S., Volk, K., & Bidelman, W. P. 1997, ApJS, 112, 557

Kwok, S. 1993, ARA&A, 31, 63

Lepine, J. R. D., Ortiz, R., & Epchtein, N. 1995, A&A, 299, 453

Lewis, B. M., Kopon, D. A., & Terzian, Y. 2004, AJ, 127, 501

Lewis, B. M. 2002, ApJ, 576, 445

Lewis, B. M. 1992, ApJ, 396, 251

Lewis, B. M., Eder, J., Terzian, Y. 1990, ApJ, 362, 634

Olnon, F. M., Baud, B., Habing, H. J., de Jong, T., Harris, S., & Pottasch, S. R. 1984, ApJ (Letters) 278, 41

Perea Calderon, J.V., García-Lario, P., Jiménez-Esteban, F. M., & Suárez, O. 2005, in preparation

te Lintel Hekkert, P., Caswell, J. L., Habing, H. J., Haynes, R. F., Haynes, R. F., & Norris, R. P. 1991, A&AS, 90, 327

Wendker, H. J. 1995, A&AS, 109, 177

Whitelock, P., Menzies, J., Feast, M., et al. 1994, MNRAS, 267, 711

Zijlstra, A. A., Te Lintel Hekkert, P., Pottasch, S. R., Caswell, J. L., Ratag, M., & Habing, H. J. 1989, A&A, 217, 157